第 35 卷第 5 期
2019 年 5 月

无 机 化 学 学 报
CHINESE JOURNAL OF INORGANIC CHEMISTRY

Vol.35 No.5
915-922

Cr^{3+}和 Ni^{2+}复合掺杂的尖晶石氧化物用于提高钻孔热电池放电性能

宋恒旭 牛永强 赵宇宏* 连冬晓 任敬霞 张妍妍 侯 华
(中北大学材料科学与工程学院,太原 030051)

摘要:为了提高用于油气以及地热钻井热电池正极材料的比容量和电压稳定性,将 Cr 和 Ni 离子同时掺杂到尖晶石锰酸锂中。通过固相法制备的 $LiCr_xNi_yMn_{2-x-y}O_4$($0\leqslant x\leqslant 0.3$,$0\leqslant y\leqslant 0.3$)材料显示出结晶度良好的尖晶石相结构和规则的八面体形态。研究了 $LiCr_xNi_yMn_{2-x-y}O_4$ 材料与 $LiNO_3$-KNO_3 共晶电解质的热相容性以及 $LiCr_xNi_yMn_{2-x-y}O_4$/Li-Mg-B 电池体系在 10~30 mA·cm^{-2} 的电流密度以及 200~300 ℃的温度范围内的放电性能。用 Cr^{3+}和 Ni^{2+}部分取代尖晶石中的锰,增强了尖晶石结构的稳定性,从而提高电池的电压和容量。其中,$LiCr_{0.1}Ni_{0.3}Mn_{1.6}O_4$ 在 10 mA·cm^{-2} 和 300 ℃的条件下具有最大比容量 713.29 mAh·g^{-1},在 $LiNO_3$-KNO_3 熔盐电池中放电性能良好。

关键词:热电池;复合掺杂;尖晶石型锰酸锂;放电性能;钻孔应用
中图分类号:TM911.16 **文献标识码**:A **文章编号**:1001-4861(2019)05-0915-08
DOI:10.11862/CJIC.2019.118

Cr^{3+} and Ni^{2+} Co-doped Spinel Oxide Cathode with Improved Capacity and Voltage Stability in Thermal Battery for Geothermal Borehole

SONG Heng-Xu NIU Yong-Qiang ZHAO Yu-Hong*
LIAN Dong-Xiao REN Jing-Xia ZHANG Yan-Yan HOU Hua
(*School of Materials Science and Engineering, North University of China, Taiyuan* 030051, *China*)

Abstract: In order to enhance specific capacity and voltage stability of cathode material for thermal battery used in oil/gas and geothermal boreholes, Cr and Ni ions were doped into spinel lithium manganate simultaneously. The $LiCr_xNi_yMn_{2-x-y}O_4$ ($0\leqslant x\leqslant 0.3$, $0\leqslant y\leqslant 0.3$) material prepared by solid-state method showed a good purity of spinel phase and a regular octahedral crystalline particles morphology. We investigated the thermal compatibility of the $LiCr_xNi_yMn_{2-x-y}O_4$ material with $LiNO_3$-KNO_3 eutectic electrolyte and the discharge performance of $LiCr_xNi_yMn_{2-x-y}O_4$/Li-Mg-B battery system at current densities from 10 to 30 mA·cm^{-2} over a temperature range of 200 to 300 ℃. Partial substitution of Cr^{3+} and Ni^{2+} for Mn in spinel improved battery voltage and capacity due to the enhanced stability of spinel structure, and the $LiCr_{0.1}Ni_{0.3}Mn_{1.6}O_4$ had the maximal specific capacity of 713.29 mAh·g^{-1} at 10 mA·cm^{-2} at 300 ℃, showing great potential in $LiNO_3$-KNO_3 molten salt battery for geothermal borehole applications.

Keywords: thermal battery; co-doping; spinel lithium manganate; discharge performance; borehole application

0 Introduction

Thermal batteries have been widely used in the military since they were invented during World War II[1]. The thermal battery as a reserve battery can be stored for decades because its electrolyte is a poor ionic and electronic solid salt at ambient temperature. The battery function only when the solid salt electrolyte

收稿日期:2018-12-03。收修改稿日期:2019-03-28。
国家自然科学基金(No.51774254,51774253,51701187,U1610123,51674226,51574207,51574206,51804279,51801189)和山西省科技重大专项(MC2016-06)资助。
*通信联系人。E-mail:zhaoyuhong@nuc.edu.cn

becomes molten, so it is suitable for working in high temperature environments. Recently, a considerable amount of work has been done to apply the principle of thermal batteries to geothermal exploration and oil/gas drilling. As we know, the typical electrolyte of thermal battery such as LiCl-KCl eutectic has a melting point as high as 352 ℃[2], while the environments of geothermal and oil/gas boreholes have a temperature usually below 300 ℃[3]. It is necessary to modify the thermal battery system to adapt to lower temperature applications. In recent years, there has been increasing activity using the nitrate electrolyte system based on its lower melting point, for example, the composition with 33.21% (*w*/*w*) $LiNO_3$-66.79% (*w*/*w*) KNO_3 nitrate salt melts at 124.5 ℃[4].

Since the conventional sulfide cathode materials are not compatible with molten nitrates, a considerable amount of work has been done to screen suitable candidate cathode materials and oxides are considered suitable alternatives[5]. Ag_2CrO_4 as a cathode material has been reported with Li-Al anode and nitrate electrolyte between 160 to 215 ℃ by Giwa[6]. After that, Guidotti et al. examined Ag_2CrO_4[7], $LiMn_2O_4$[8], MnO_2[3,8], CrO_2, and $LiCoO_2$ with lithium alloy anode and KNO_3-$LiNO_3$ eutectic electrolyte over a wider temperature range. More recently manganese oxides have been increasing attention because they exhibit not only large specific capacity but also environment-friendly. Niu et al. studied the electrochemical behavior of MnO_2 cathode material in various nitrate electrolyte systems over a temperature range of 150 to 300 ℃ and current densities from 10 to 30 $mA \cdot cm^{-2}$ [9-12]. Meanwhile, Wang et al. examined the discharge performance of lithium manganese oxide and their derivatives by doped Ni[13] and Co[14] with lithium alloy anode and KNO_3-$LiNO_3$ eutectic electrolyte. A more stable voltage plateau and a larger specific capacity can be obtained by doping in $LiMn_2O_4$, and we increased the specific capacity and improved its rate performance by doping chromium into $LiMn_2O_4$ in previous work[15].

In order to enhance specific capacity and voltage stability of cathode material, Cr and Ni ions were introduced into spinel lithium manganate simultaneously. This material was used as a cathode material for rechargeable lithium-ion batteries at room temperature[16-17], but has not been reported at higher temperatures as far as we know. Here, we reported the material characteristics of chromium-nickel substituted spinel oxide materials and analyzed their discharge performance in single batteries over a temperature range of 200 to 300 ℃.

1 Experimental

1.1 Materials preparation

For the preparation of spinel $LiCr_xNi_yMn_{2-x-y}O_4$ ($0 \leqslant x \leqslant 0.3$, $0 \leqslant y \leqslant 0.3$) material, stoichiometric amounts of $LiOH \cdot H_2O$ (95.0%(*w*/*w*), Fengchuan, China), Cr_2O_3 (99.0% (*w*/*w*), Sinopharm, China), NiO (99.0% (*w*/*w*), Aladdin, China) and MnO_2 (>97.5% (*w*/*w*), Sangon Biotech, China) powders were mixed and ground using a planetary ball-milling machine (Nanjing Nanda Instrument Plant, QM-3SP4, China). After this, the powders were precalcined at 470 ℃ for 6 h, then heated to the temperature of 600 ℃ for 6 h and 750 ℃ for 12 h in a resistance furnace in an air atmosphere. The precipitates were then natural cooling of the resistance furnace to room temperature and finally through grinding and sieving.

The separator mix consisted of 65%(*w*/*w*) $LiNO_3$-KNO_3 eutectic electrolyte and 35%(*w*/*w*) MgO powder (>98% (*w*/*w*), BBI Life Sciences, China), where the MgO powder was used as a binding agent to resist electrolyte flow when it melted. The preparation method of separator mix refered to Guidotti's report[7]. The catholyte consisted of 70%(*w*/*w*) of the active cathode material, 20%(*w*/*w*) $LiNO_3$-KNO_3 electrolyte and 10% (*w*/*w*) graphite powder (>99%(*w*/*w*), Sangon Biotech, China). Graphite powder was added to improve the conductivity of the cathode material because the conductivity of the lithium manganate material was poor. The anolyte consisted of Li-Mg-B alloy (58%, 4% and 38%(*w*/*w*), respectively).

1.2 Material characterization

The crystalline structures of the spinel $LiCr_xNi_yMn_{2-x-y}O_4$ ($0 \leqslant x \leqslant 0.3$, $0 \leqslant y \leqslant 0.3$) materials were carried out on a X-ray diffractometer (XRD,

Rigaku D/max-Rb, Japan) with Cu $K\alpha_1$ radiation (λ= 0.154 08 nm) in a 2θ range of 15°~85° at the speed of 2°·min^{-1}. The XRD instrument was operated at accelerating voltage of 40 kV and current of 100 mA. The morphologies of the samples were performed by a field emission scanning electron microscopy (FESEM; Zeiss merlin compact, Germany) operated at 10 kV. The thermal stabilities and compatibilities of the materials were analyzed by a simultaneous differential scanning calorimetry (DSC, Netzsch STA 449 C, Germany) and thermogravimetric analysis (TGA). The samples powder were sealed in Al_2O_3 pans and were heated at a rate of 10 K·min^{-1} from room temperature to 500 ℃ in high-purity argon atmosphere.

1.3 Single-cell testing

The single cell was constructed with anolyte, separator mix, catholyte and current collectors. The anolyte pellet was punched into a diameter of 16 mm, thickness of 1 mm, and mass of 0.188 g wafer by a die. While the separator mix (0.2 g) and catholyte (0.2 g) powders were placed by layer in a die and pressing them to a pellet with a pressure of 14 MPa. Finally, 304 stainless steel of current collectors and the two electrode pellets were combined into a single cell with sandwich structure.

The discharge performance of the single cell was measured by an electrochemical test instrument (CT-4008, Neware Technology Co. Ltd., China). Steady-state currents of 19 to 57 mA (10 to 30 mA·cm^{-2}, respectively) were loaded on the single cell at a temperature of 200 to 300 ℃. The discharge of the single cell was terminated when the voltage dropped below 1.00 V. It should be noted that above preparations, processing, and handling operations with materials and cells were conducted in a glovebox with an atmosphere of high-purity argon (The volume fraction of water and oxygen is less than 1×10^{-6}).

2 Results and discussion

2.1 XRD analysis

Fig.1 shows the XRD patterns of the spinel $LiCr_xNi_yMn_{2-x-y}O_4$ ($0\leqslant x\leqslant0.3$, $0\leqslant y\leqslant0.3$) samples. As can be seen from Fig.1 that the diffraction peaks of spinel samples with different doping amounts were well consistent with the characteristic peaks of $LiMn_2O_4$ (PDF No.70-3120) with an *Fd*3*m* space group. No additional diffraction peaks were observed except for lithium manganate, indicating a good purity of the spinel samples. It can be clearly observed that the diffraction peaks of the doped derivative were shifted to a large angle compared to $LiMn_2O_4$ according to the partial enlargement of the (400) plane diffraction peak, which was caused by the decrease of lattice parameters due to doping. As we know, the average oxidation states of manganese ions in $LiMn_2O_4$ is +3.5, that is, the amount of Mn^{3+} and Mn^{4+} ions exist in a ratio of 1:1. X-ray photoelectron spectrometry (XPS) analysis show that the oxidation states of Cr and Ni in lithium manganate are +3 and +2, respectively[17], and the two ions have a radius of 0.061 5 and 0.070 nm, respectively. Both of Cr^{3+} and Ni^{2+} ions substitute the Mn^{3+} ions in lithium manganate, thus the Mn^{3+} ions (0.064 5 nm) shift to the smaller radius of the Mn^{4+} ions (0.053 nm) with the addition of Ni^{2+} ions in order to maintain electrical neutrality. The lattice parameters of the spinel sample calculated based on the XRD diffraction data are listed in Table 1, and this result is consistent with the above discussion. However, the sample with the most doped amount of Ni^{2+} ions did not have the smallest interplanar spacing, which may be related to the loss of oxygen in the sample.

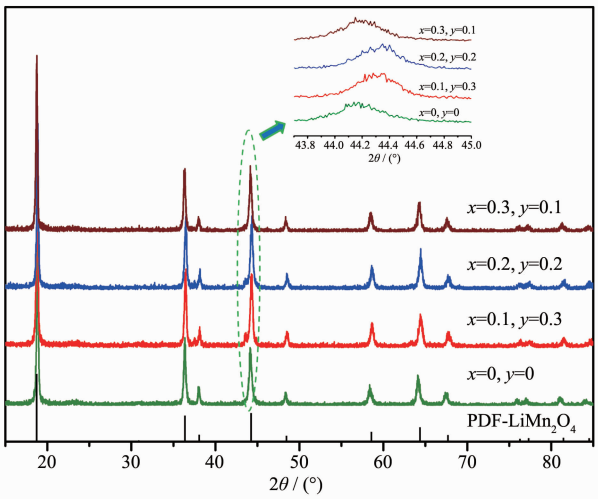

Fig.1 XRD patterns of the spinel $LiCr_xNi_yMn_{2-x-y}O_4$ ($0\leqslant x\leqslant0.3$, $0\leqslant y\leqslant0.3$) samples

Table 1 Structure parameters of $LiCr_xNi_yMn_{2-x-y}O_4$ ($0 \leqslant x \leqslant 0.3$, $0 \leqslant y \leqslant 0.3$) samples

Sample	Lattice parameter / nm	Unit cell volume / nm^3
$LiMn_2O_4$	0.820 230	0.551 83
$LiCr_{0.1}Ni_{0.3}Mn_{1.6}O_4$	0.817 276	0.545 89
$LiCr_{0.2}Ni_{0.2}Mn_{1.6}O_4$	0.816 871	0.545 08
$LiCr_{0.3}Ni_{0.1}Mn_{1.6}O_4$	0.819 629	0.550 62

2.2 SEM images

Fig.2 shows SEM images of the spinel $LiCr_xNi_yMn_{2-x-y}O_4$ ($0 \leqslant x \leqslant 0.3$, $0 \leqslant y \leqslant 0.3$) with different dopants. As shown in Fig.2a, the undoped $LiMn_2O_4$ powder had a relatively uniform particle size about 200 nm and an irregular granular shape of surface morphology. While the lithium manganate materials doped with chromium and nickel all exhibited as regular octahedral crystalline particles, and the particle size became uneven compared to the undoped lithium manganate materials, that is, larger particles began to appear. It can be further observed that $LiCr_{0.2}Ni_{0.2}Mn_{1.6}O_4$ sample showed the largest particle size non-uniformity from Fig.2c. According to report by Kang et al.[18], octahedral morphology with good crystallinity contributes to the improvement of the thermal stability of the materials, which is consistent well with the discharge performance of the single cell.

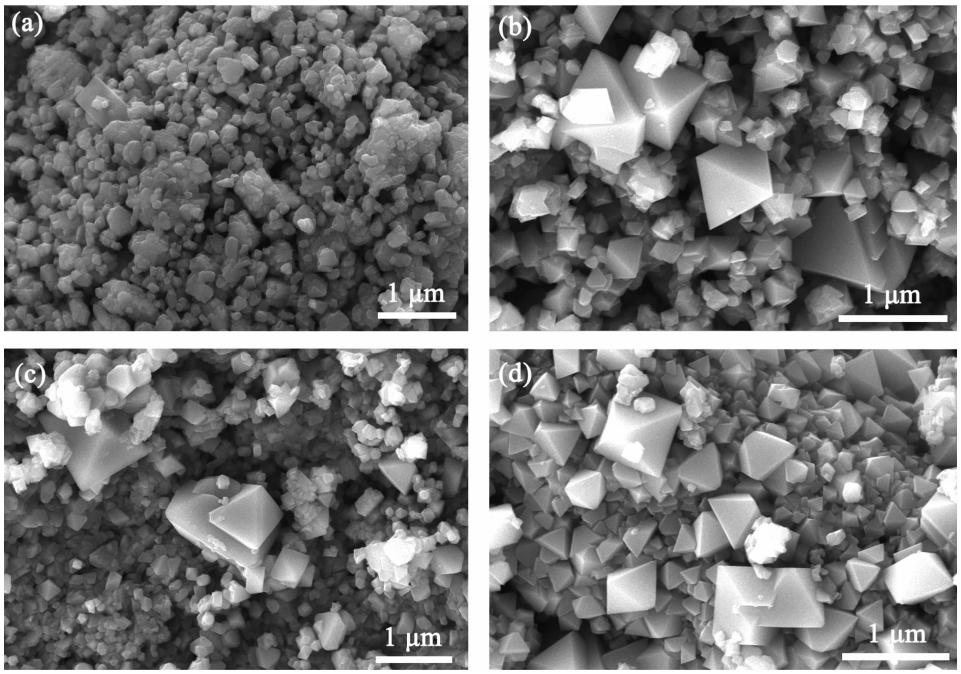

Fig.2 SEM images of (a) $LiMn_2O_4$, (b) $LiCr_{0.1}Ni_{0.3}Mn_{1.6}O_4$, (c) $LiCr_{0.2}Ni_{0.2}Mn_{1.6}O_4$ and (d) $LiCr_{0.3}Ni_{0.1}Mn_{1.6}O_4$ powders prepared by solid state method

2.3 Thermal analyses

In order to characterize the thermal stability of the spinel samples, the $LiCr_{0.2}Ni_{0.2}Mn_{1.6}O_4$ was analyzed by DSC and TG, and the result was shown in Fig.3. No obvious endothermic or exothermic peak was observed from the DSC curve from room temperature to 500 ℃. From the TG curve, no weight loss was observed during the heating process, except for the weight loss caused by the atmospheric fluctuation at the beginning. The result indicates that the prepared active cathode material has a good thermal stability.

To characterize the thermal compatibility between the spinel samples with the $LiNO_3$-KNO_3 eutectic electrolyte and the thermal stability of the catholyte material, the catholyte material containing 70% (*w*/*w*) $LiCr_{0.2}Ni_{0.2}Mn_{1.6}O_4$, 10% (*w*/*w*) graphite, and 20% (*w*/*w*) electrolyte were analyzed by DSC and TG and the result was shown in Fig.4. As can be seen from the

TG curve in Fig.4, only one major endotherm at 130.9 ℃, which can be assigned to the melting of the $LiNO_3$-KNO_3 electrolyte. In Guidotti′s report, the melting point of $LiNO_3$-KNO_3 eutectic electrolyte is 124.5 ℃[19]. This difference is mainly due to the fact that the test samples in this work are not pure $LiNO_3$-KNO_3 eutectic electrolyte. From the TG curve, no obvious weight loss was observed from room temperature to 400 ℃, however, the weight loss began to apparent at temperatures higher than 400 ℃, which is caused by the thermal decomposition of nitrates electrolyte accompanied by the generation of O_2[12].

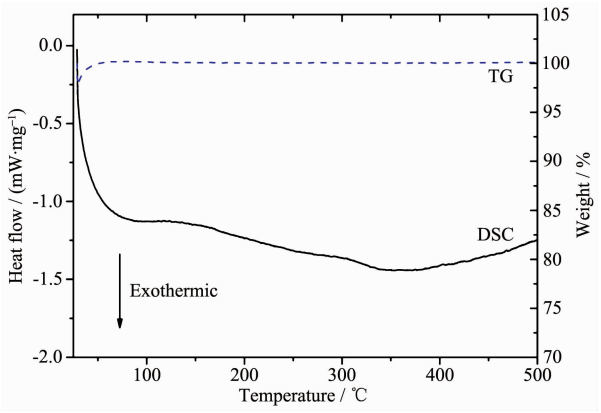

Fig.3　DSC and TG curves of spinel $LiCr_{0.2}Ni_{0.2}Mn_{1.6}O_4$ sample

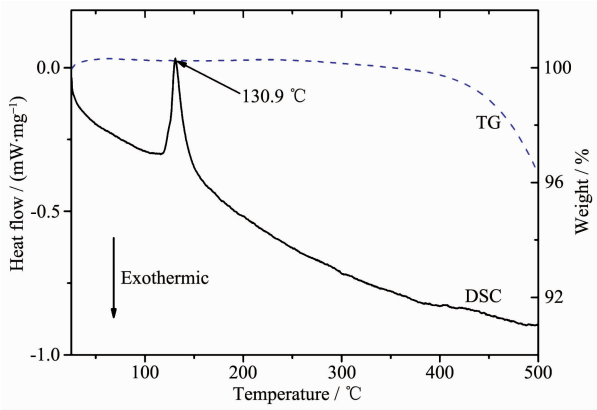

Fig.4　DSC and TG curves of the catholyte material containing 70%(*w*/*w*) $LiCr_{0.2}Ni_{0.2}Mn_{1.6}O_4$, 10%(*w*/*w*) graphite, and 20%(*w*/*w*) $LiNO_3$-KNO_3 electrolyte

The thermal compatibility between the $LiNO_3$-KNO_3 eutectic electrolyte and the Li-Mg-B anolyte has been reported by Niu et al[10]. Here, three endothermic events on the DSC curve corresponded to the impure phase, the melting of $LiNO_3$-KNO_3 electrolyte and the melting of lithium, respectively. In addition, no obvious exothermic event was observed from room temperature to 450 ℃.

Based on the above results, the safe operating temperature of this battery system can reach 400 ℃, which has met our needs of the battery operating temperature from 200 to 300 ℃.

2.4　Single-cell testing

Fig.5 shows the galvanostatic discharge behavior of the $LiCr_xNi_yMn_{2-x-y}O_4$/Li-Mg-B single battery with a constant current of 10 mA·cm^{-2} at a temperature of 200 ℃. It can be seen from Fig.5 that there were three distinct discharge plateaus (2.75~2.70 V, 2.30~2.10 V, 1.70~1.50 V, respectively.) during discharge. It was noteworthy that the voltage of the undoped lithium manganate was slight higher than that of the doped lithium manganate at the initial discharge, however, the voltage of the undoped lithium manganate was lower than that of the doped lithium manganate at the second and third voltage plateaus about 0.2 and 0.3 V, respectively. Samples doped with chromium and nickel have almost the same discharge plateaus, and $LiCr_{0.3}Ni_{0.1}Mn_{1.6}O_4$ had the largest discharge capacity of 585.14 mAh·g^{-1} when the discharge voltage dropped to 1.0 V.

Fig.6 shows the galvanostatic discharge behavior of the $LiCr_xNi_yMn_{2-x-y}O_4$/Li-Mg-B single battery at a higher current density of 30 mA·cm^{-2} at a temperature

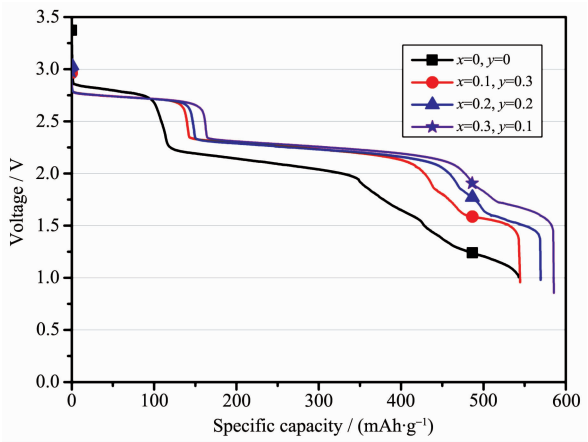

Fig.5　Galvanostatic discharge behavior of the $LiCr_xNi_yMn_{2-x-y}O_4$/Li-Mg-B single battery with a constant current of 10 mA·cm^{-2} at a temperature of 200 ℃

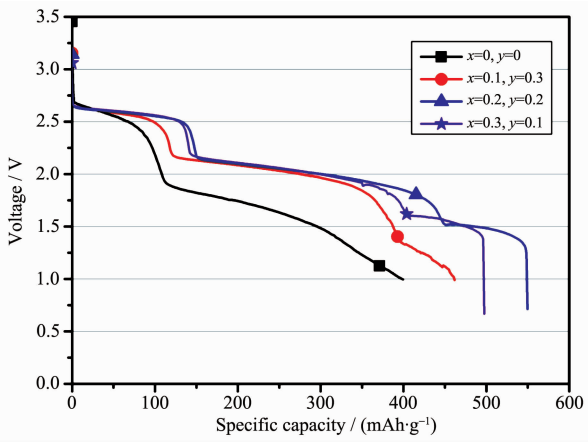

Fig.6 Galvanostatic discharge behavior of the $LiCr_xNi_yMn_{2-x-y}O_4$/Li-Mg-B single battery with a constant current of 30 mA·cm^{-2} at a temperature of 200 ℃

of 200 ℃. As shown in Fig.6, the galvanostatic discharge profiles were similar to the condition at 10 mA·cm^{-2}, there were also three distinct discharge plateaus during discharge. The first and second voltage plateaus of the doped lithium manganate were at the ranges of 2.50~2.65 and 1.75~2.15 V respectively, while the third voltage plateau had a significant difference in doping levels. It is obvious that samples doped with chromium and nickel outperformed undoped lithium manganate in both voltage and capacity. The reasons for such excellent discharge performance of chromium and nickel co-doping materials are listed as follows: First, the binding energies of Cr-O and Ni-O in MO_2 are 1 142 and 1 029 kJ·mol^{-1}, respectively, which is stronger than the binding energy of Mn-O of 946 kJ·mol^{-1} [20-21]. Therefore, the doping of Cr and Ni enhances the stability of lithium manganate spinel structure. Second, the partial substitution of Cr^{3+} and Ni^{2+} for Mn^{3+} reduces the trivalent Mn^{3+} ions in spinel, which alleviates the local distortion in MnO_6 octahedrons consisting of the spinel structure[22]. Third, as we mentioned above in the SEM section, a good crystallinity octahedral structure obtained by doping Cr and Ni is more favorable for the thermal stability of the material. Compared with the condition at 10 mA·cm^{-2}, the overall performance including voltage and capacity of the battery system decreased at 30 mA·cm^{-2}, which could be attributed to the poor electrical conductivity of the spinel material. Notably, the $LiCr_{0.2}Ni_{0.2}Mn_{1.6}O_4$ had the largest discharge capacity of 549.57 mAh·g^{-1} when the discharge voltage dropped to 1.0 V, which was higher than 37.6% of undoped original spinel oxide (399.5 mAh·g^{-1}). This result indicates that partial substitution of chromium and nickel for manganese is more effective to improve the cell performance at higher currents.

In order to further investigate the discharge performance of the $LiCr_xNi_yMn_{2-x-y}O_4$/Li-Mg-B cell at a higher temperature, the single cell was designated to discharge at 300 ℃ at a constant current density of 10 and 30 mA·cm^{-2}, as shown in Fig.7 and 8, respectively. Compared with the condition at 200 ℃, the discharge curves also presented three voltage plateaus, the difference being that the second and third voltage platforms differ less, which was especially noticeable at lower current densities of 10 mA·cm^{-2} (Fig.7). As shown in Fig.7, the initial discharge plateau was stable in the range of 2.60~2.75 V, while the subsequent voltage platform exhibited a large voltage difference with the doping amount. This result may be mainly cause by an increase in unexpected side reactions at high temperatures, resulting in a degradation of voltage stability. In terms of capacity, the battery system had an outstanding performance under this condition, and the $LiCr_{0.1}Ni_{0.3}Mn_{1.6}O_4$ had the largest discharge capacity of 713.29 mAh·g^{-1}, even the undoped

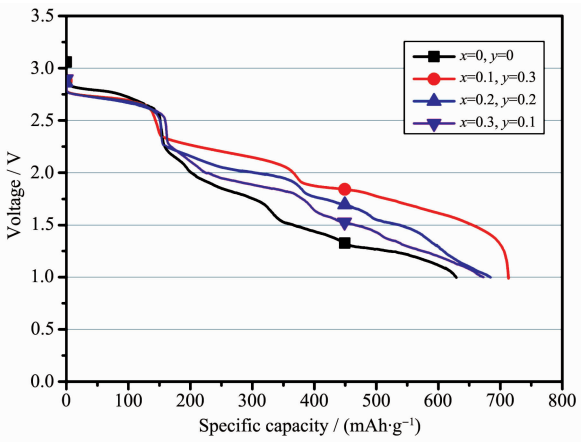

Fig.7 Galvanostatic discharge behavior of the $LiCr_xNi_yMn_{2-x-y}O_4$/Li-Mg-B single battery with a constant current of 10 mA·cm^{-2} at a temperature of 300 ℃

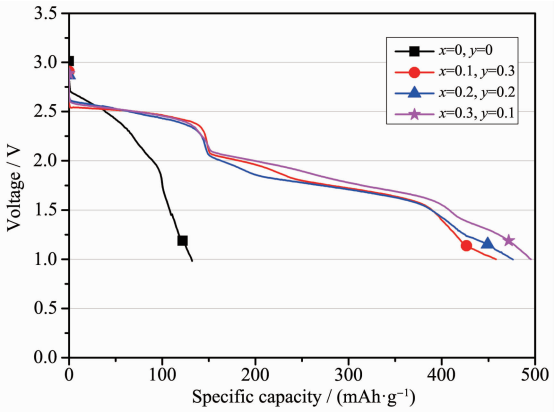

Fig.8　Galvanostatic discharge behavior of the $LiCr_xNi_yMn_{2-x-y}O_4$/Li-Mg-B single battery with a constant current of 30 mA·cm^{-2} at a temperature of 300 ℃

original spinel had a specific capacity of 629.07 mAh·g^{-1}. This is due to the improvement of good electrolyte conductivity at high temperatures. The main reason for the increase of discharge capacity is attributed to the higher ionic conductivity of the electrolyte by enhanced kinetics at higher temperature.

We found that the double ion doped spinel materials have better discharge performance than the single ion doped spinel materials under this condition. For example, the specific capacity of $LiNi_{0.3}Mn_{1.7}O_4$[13] and $LiCr_{0.1}Mn_{1.9}O_4$[15] spinel under the same conditions are 335.95 and 614.29 mAh·g^{-1} respectively, which is much lower than that of $LiCr_{0.1}Ni_{0.3}Mn_{1.6}O_4$ of 713.29 mAh·g^{-1} in this work, and the main reason for this result may be the synergistic action of the two ions.

From Fig.8, it can be seen that the original $LiMn_2O_4$ sample exhibited poor discharge performance at a higher current density of 30 mA·cm^{-2} at a temperature of 300 ℃. After partial substitution of Mn in lithium manganate with Cr and Ni, the discharge specific capacity of the battery has been dramatically improved from the original 132.00 mAh·g^{-1} to the highest 495.43 mAh·g^{-1} ($LiCr_{0.1}Ni_{0.3}Mn_{1.6}O_4$).

3　Conclusions

Cr and Ni doped spinel $LiCr_xNi_yMn_{2-x-y}O_4$ ($0 \leqslant x \leqslant 0.3$, $0 \leqslant y \leqslant 0.3$) cathode materials have been successfully synthesized through solid-state method and maintained the *Fd*3*m* spatial structure of the spinel which has been confirmed by XRD results. Partial substitution of Cr^{3+} and Ni^{2+} for Mn in spinel improves battery voltage and capacity at current densities from 10 to 30 mA·cm^{-2} over a temperature range of 200 to 300 ℃. The $LiCr_xNi_yMn_{2-x-y}O_4$/Li-Mg-B battery system had the most outstanding discharge performance at a constant current density of 10 mA·cm^{-2} at 300 ℃, and the $LiCr_{0.1}Ni_{0.3}Mn_{1.6}O_4$ had the maximal specific capacity of 713.29 mAh·g^{-1}. The dramatic improvement in discharge performance of the battery system is mainly because that the doping of chromium and nickel enhanced the structural stability of spinel lithium manganate oxides. Based on the stable structure of the material, the battery has a more significant improvement in discharge performance at higher current densities, in other words, doping makes the battery have better rate discharge performance. In addition, it should be noted that the discharge performance of the battery in different environments depends on the amount of dopant.

Based on the above results and discussion, the $LiCr_xNi_yMn_{2-x-y}O_4/LiNO_3$-$KNO_3$/Li-Mg-B battery system was evaluated suitable for using as a power supply for geothermal borehole applications.

Acknowledgements: This work was supported by the National Natural Science Foundation of China (Grants No. 51774254, 51774253, 51701187, U1610123, 51674226, 51574207, 51574206, 51804279, 51801189) and the Science and Technology Major Project of Shanxi Province (Grant No. MC2016-06).

References:

[1] Guidotti R A, Masset P. *J. Power Sources*, **2006**,**161**:1443-1449

[2] Guidotti R A, Reinhardt F W. *Progress in Electrochemical Society Meeting*. San Francisco: [s.n.], **1994**.

[3] Guidotti R A, Reinhardt F W. 41*st Power Sources Conference*. Philadelphia: [s.n.], **2004**.

[4] Guidotti R A, Normann R A, Reinhardt F W, et al. *Trans.-Geotherm. Resour. Counc.*, **2003**,**27**:1-9

[5] SONG Heng-Xu(宋恒旭), NIU Yong-Qiang(牛永强), HOU Hua(侯华), et al. *Chinese J. Inorg. Chem.*(无机化学学报), **2017**,**33**:2155-2168

[6] Giwa C O. *Materials Science Forum*: *Vol.*73-75. Chemla M, Devilliers D, Vogler M. Ed., Zurich: Trans Tech Publication Ltd., **1991**:699-706

[7] Guidotti R A, Reinhardt F W. 201*st Electrochemical Society Meeting*. Albuquerque: Sandia National Laboratories, **2002**.

[8] Guidotti R A, Reinhardt F W. *IBA*-2000 *Manganese Oxide Battery Symposium*. Albuquerque: Sandia National Laboratories, **2001**.

[9] Niu Y Q, Wu Z, Du J L. *J. Electrochem. Soc*., **2013**,**160**: A1375-A1379

[10]Niu Y Q, Wu Z, Du J L, et al. *J. Power Sources*, **2014**,**245**: 537-542

[11]Niu Y Q, Wu Z, Du J L, et al. *Electrochim. Acta*, **2014**,**115**: 607-611

[12]Niu Y Q, Wu Z, Du J L, et al. *Solid State Ionics*, **2014**,**255**: 80-83

[13]Wang Z J, Du J L, Duan W Y, et al. *Int. J. Electrochem. Sci.*, **2013**,**8**:6231-6242

[14]Wang Z J, Du J L, Li Z L, et al. *Ceram. Int.*, **2014**,**40**:3527-3531

[15]Song H X, Zhao Y H, Niu Y Q, et al. *Solid State Ionics*, **2018**,**325**:67-73

[16]Rajakumar S, Thirunakaran R, Sivashanmugam A, et al. *J. Electrochem. Soc.*, **2010**,**157**:A333-A339

[17]Chen D R, Li B Z, Liao Y H, et al. *J. Solid State Electrochem.*, **2014**,**18**:2027-2033

[18]Kang Y J, Kim J H, Sun Y K. *J. Power Sources*, **2005**,**146**: 237-240

[19]Guidotti R A. 35*th Intersociety Energy Conversion Engineering Conference and Exhibit*: *Vol.*2. New York: IEEE, **2000**:1276-1286

[20]Li G H, Ikuta H, Uchida T, et al. *J. Electrochem. Soc.*, **1996**,**143**:178-182

[21]Yi T F, Xie Y, Ye M F, et al. *Ionics*, **2011**,**17**:383-389

[22]Okumura T, Fukutsuka T, Matsumoto K, et al. *J. Phys. Chem. C*, **2011**,**115**:12990-12994